Electronic Supplementary Information

Perovskite $CoSn(OH)_6$ nanocubes with tuned d-band states towards enhanced oxygen evolution reactions

Mingwei Sun, [a, b] Baopeng Yang, [c] Jiaxing Yan, [b] Yulong Zhou, [b] Zhencong Huang, [b] Ning Zhang, *, [b] Rong Mo, *, [a] and Renzhi Ma *, [d]

[a] Hunan Key Laboratory for Micro-Nano Energy Materials and Devices, School of Physics and Optoelectronics, Xiangtan University, Hunan 411105, P. R. China

[b] School of Materials Science and Engineering, Central South University, Changsha 410083, China

[c] School of Physics and Electronics, Central South University, Changsha 410083, China

[d] Research Center for Materials Nanoarchitectonics (MANA), National Institute for Materials Science (NIMS), 1-1 Namiki, Tsukuba, Ibaraki 305-0044, Japan

* Corresponding authors: Ning Zhang (nzhang@csu.edu.cn); Rong Mo (morong@xtu.edu.cn)；Renzhi Ma (ma.renzhi@nims.go.jp).

1. DFT computational details.

In this study, all theoretical calculations were carried out by the Vienna ab-initio Simulation Package (VASP) based on the density functional theory (DFT). The generalized gradient approximation (GGA) in the form of Perdew-Burke-Ernzerhof (PBE) exchange-correlation functional was used to describe the electron exchange-correlation. The interaction between electron and ion was treated by the projector augmented wave (PAW) method. For all calculations, the cut-off energy was set to be 520 eV, the convergence criterion for the self-consistent field energy was set to be 1.0×10^{-4} eV, and the final force on each atom was less than 0.05 eV/Å for each ionic step. A Gamma k-point mesh of 3×3×1 was used. Grimme's DFT-D3 method was incorporated to implement the van der Waals correction. The calculated models are shown in Figure S8. In this work, (001) surface of these catalysts was constructed to simulate reaction interface, the vacuum thickness was set to be 20 Å to minimize interlayer interactions. The calculated model includes two octahedral layers, containing six Co (or Fe) atoms, six Sn atoms and thirty-six O atoms. During calculations, the bottom two layers were fixed, but the top one layer was relaxed.

The OER on catalyst surface was simulated according to the following reactions:

$$*+4OH^- \rightarrow *OH + 3OH^- + e^-$$

$$*OH + 3OH^- + e^- \rightarrow *O + H_2O + 2OH^- + 2e^-$$

$$*O + H_2O + 2OH^- + 2e^- \rightarrow *OOH + H_2O + OH^- + 3e^-$$

$$*OOH + H_2O + OH^- + 3e^- \rightarrow *+ O_2 + 2H_2O + 4e^-$$

Here, (*) represent the adsorption site. The free energy change (ΔG) of each elementary reaction was calculated as follows:

$$\Delta G = \Delta E + \Delta ZPE - T \times \Delta S$$

where ΔE is the difference of electronic energy between products and reactants, ΔZPE is the change of zero-point energies, and ΔS is the entropy change.

2. Chemicals. Sodium stannate (Na_2SnO_3, Analytical Reagent), cobalt chloride hexahydrate ($CoCl_2\cdot6H_2O$, Analytical Reagent), iron chloride hexahydrate ($FeCl_3\cdot6H_2O$, AR, 99%), and potassium hydroxide (KOH, ACS) were purchased from

Aladdin Industrial Corporation. Nafion *D-521 dispersion (5% w/w in water and 1-propanol, ⩾ 0.92 meq/g exchange capacity) was produced from Alfa Aesar chemical Co. Ltd. All reagents were used as received without further purifying. Deionized water (DI) was used for the synthesis of all samples.

3. Synthesis of $CoSn(OH)_6$, and $CoSn(OH)_6$ electrocatalysts.

Nanocrystals of perovskite hydroxide $CoSn(OH)_6$ were prepared by a hydrothermal method. In a typical procedure, Na_2SnO_3 (1.0 mmol) and $CoCl_2 \cdot 6H_2O$ (1.5 mmol) were dissolved in 20 mL deionized water separately. Then, above solutions were mixed and stirred for 10 min. Afterward, the mixed solution was transferred into a sealed Teflon-lined stainless-steel autoclave and subsequently heated on electronic oven at 200 °C for 24 h. After cooling to room temperature, the products were washed several times using distilled water and ethanol. Finally, the products were dried at 60 °C for 12 h. The obtained powders were collected and ground into a fine powder.

4. Synthesis of CoFe-LDH electrocatalysts.

CoFe-LDH was prepared by a hydrothermal method. Typically, $Co(NO_3)_2 \cdot 6H_2O$ (0.982 mmol), $Fe(NO_3)_3 \cdot 9H_2O$ (0.018 mmol), urea (5 mmol), and NH_4F (2 mmol) were dissolved in DI water (18 mL) to form a precursor solution. Subsequently, the prepared solution was transferred into a Teflon-lined (23 mL) stainless steel vessel. After that, maintained at 200 °C for 24 h. After cooling to room temperature, the CoFe-LDH on NF was rinsed with DI water and ethanol, and then dried at 60 °C for 12 h.

5. Characterizations.

X-Ray Diffraction (XRD) patterns were collected on a RIGAKU Rint-2000 X-ray diffractometer equipped with graphite monochromatized Cu-Kα radiation (λ=1.54184Å). The scanning electron microscope (SEM) images and energy-dispersive spectra were collected by the JSM-7610FPlus (Jeol, Japan) field emission scanning electron microscopy equipped with an energy dispersive spectrometer (ULTIM MAX 40 integrated on the SEM). Transmission electron microscopy (TEM), selected area electron diffraction (SAED), high-angle annular dark-field (HAADF)-

TEM measurements, and high-resolution transmission electron microscopy (HR-TEM) were obtained on FEI Tecnai G2 F200X field emission transmission electron microscope at an accelerating voltage of 200 kV. EDX elemental mapping was obtained using TalosTM F200X field emission transmission electron microscope at 200 kV. The X-ray photoelectron spectroscopy (XPS) was carried out on a Thermo Scientific K-Alpha spectrophotometer using an Al Kα X-ray excitation source (hv=1486.6 eV), an analysis area of 400 μm in diameter and a pass energy of 50 eV. The C 1s at 284.8 eV from adventitious carbon was used to calibrate the XPS spectra. In-situ Raman characteristics were performed using a spectroelectrochemical cell (ECC-Opto-Std-Aqu, EL-Cell GmbH, Hamburg, Germany) that uses an Ag/AgCl reference electrode. The potentials measured were converted to RHE.

6. Electrochemical measurements. The OER measurements were performed using a conventional three-electrode system using an electrochemical workstation (CHI 760D, Shanghai Chenhua Instrument Co. Ltd.). The working electrode was dry carbon fiber paper (CFP) modified with various catalysts, the counter electrode was a platinum plate (Pt, 1 cm x 1 cm), and the reference electrode was a Hg/HgO (1M KOH-filled) electrode. And the area of carbon fiber paper is fixed at 0.5 x 0.5 cm^2. For the fabrication of the working electrode, approximately 10 mg of catalyst was dispersed in 2 mL mixed solution of distilled water (1000 μL), ethanol (1000 μL) and the proton conducting binder (20 μL 5 wt % Nafion), followed by at least 60 min sonication to form a homogeneous ink. Then, 20 μL of the resulting dispersion was dropped onto a piece of dry carbon fiber paper (0.5 x 0.5 cm^2 with an electrocatalyst loading of ~0.4 mg cm^{-2}). Then the carbon fiber paper was dried in a vacuum oven at 60 °C for 24 h. All potentials were referenced to reversible hydrogen electrode (RHE) by following calculations: $E_{RHE} = E_{Hg/HgO} + 0.059 \times pH + 0.098$. The oxygen evolution reaction was evaluated by linear sweep voltammetry (LSV) between 1.0 and 1.8 V (vs. RHE) at a scan rate of 10 mV s^{-1}. Before collecting the data, cyclic voltammetry (CV) between 1.4 and 1.8 V (vs. RHE) were performed with 200 cycles to reach the stabilization at a scan rate of 30 mV s^{-1}. The current density was normalized to the geometric area (0.25 cm^2) of the carbon fiber paper. The Tafel slope was calculated according to

Tafel equation as follows: $\eta = b\log j + a$, where η is overpotential (V), j is the current density (mA cm^{-2}), and b is the Tafel slope (mV $dec^{-1)}$. To determine the electrochemical active surface area (ECSA) of different samples, a series of CV curves were collected at different scan rates (20, 40, 60, 80, 100, 120, 140 and 160 mV s^{-1}) within an appropriate potential range (1.35 V-1.45 V) where no Faradaic reaction occurred. It could be found that the relationship of the double layer current and the scan rates could be linearly fitted. The double-layer capacitance (C_{dl}) was estimated by the slope of the relationship between $\triangle j = j_a - j_c$ (j_a is the anodic current densities and j_c is the cathodic current densities at 1.40 V vs. RHE) and scan rate. The ECSA was measured and represented by C_{dl}. Electrochemical impedance spectroscopy (EIS) technique was carried out under the potential of 1.50 V (vs. RHE) in the frequency range of 0.1 Hz to 100 kHz to determine the Rs (solution resistance), R_{oad} (adsorptive or formative resistance) and R_{ct} (charge transfer resistance) of the fabricated electrode. The stability study for OER was measured by chronopotentiometry measurement at 10 mA cm^{-2} in 1 M KOH solution.

7. Photovoltaic-Electrocatalytic Water Splitting Evaluations.

The Photovoltaic-water electrolysis was characterized by an online gas chromatography (GC-2014C, Shimadzu Corp., Japan). The gas produced from water splitting reactor (Online-3, Shanghai Boyi Scientific Instrument Co., China) was collected by a closed gas-circulation system, which is connected to the online gas chromatography. Typically, the anode (the $CoSn(OH)_6$-Fe1.8% catalyst on Ni foam, 1 cm^2) and cathode (Pt plate, 1 cm^2) were installed on a water splitting reactor and connected to a crystalline silicon solar cell. Two electrodes kept around 3 cm apart. About 300 mL 1 M KOH electrolyte was placed in the water splitting reactor. Then the water splitting reactor and closed gas-circulation system were achieved vacuum state by vacuumizing. A Xe lamp with a wavelength range of 300-800 nm was used to simulate sunlight. The light intensity was controlled by the distance between solar cell and light source or adjusting the input current on Xe lamp. A crystalline silicon solar cell with a total irradiated area of 14.4 cm^2 was applied to convert photo energy to

electric energy. To protect the solar cell from overheating, a circulating water unit was placed between solar cell and light source. Moreover, the voltage from solar cell was monitored a voltmeter. The light intensity was regulated to keep a working voltage of 2.7 V from solar cell after turning on the Xe lamp.

8. Calculation of Faradaic Efficiency and solar-to-hydrogen energy conversion Efficiency.

Faraday efficiency was defined as the ratio between the actual and theoretical yield. The calculation is as following:

$$Theoretical\ gas\ yield = \frac{Q}{F \times n} = \frac{I \times t}{F \times n}$$

$$Faraday\ efficiency = \frac{actual\ gas\ yield}{Theoretical\ gas\ yield} = \frac{F \times n \times m}{I \times t} \times 100\%$$

F: the Faraday constant (96485.33289 C mol^{-1}), n: the number of electron transfer (2 for HER and 4 for OER), m: the actual moles of the product (mol), t: the reaction time (s), I: the current under voltage of 2.7 V, which is deduced by the LSV curve (Figure S13).

The solar-to-hydrogen energy conversion efficiency was defined as the ratio of the H_2 energy to the input solar energy. A spectroradiometer (AvaSolar-1, Avantes, America) was used to measure the light intensity. The calculation is as following:

$$Solar\ to\ hydrogen\ energy\ conversion\ efficiency = \frac{H_2\ energy\ (kj)}{solar\ energy\ (kj)} \times 100\%$$

H_2 energy (kj) = standard molar enthalpy of combustion (kJ mol^{-1}) × H_2 moles (mol).

Solar energy (kj) = light intensity (W cm^{-2}) × illumination area (cm^2) × time (s).

9. Additional Figures and Captions

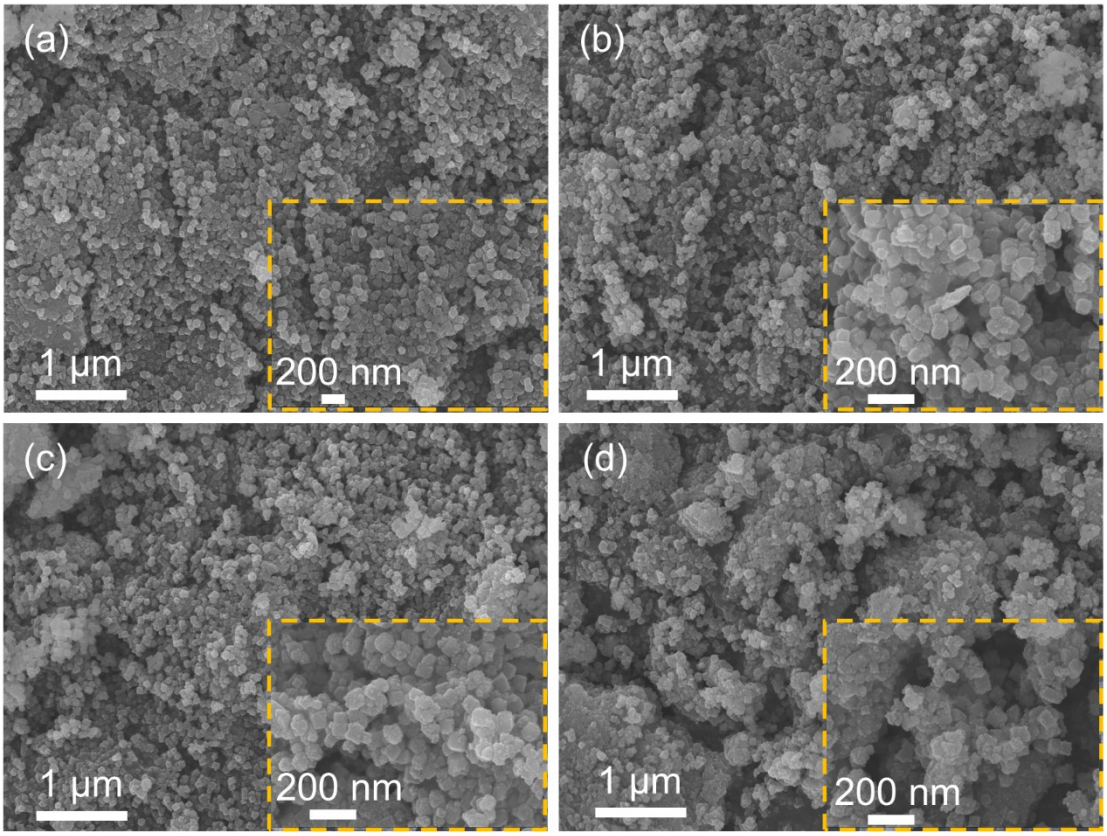

Fig. S1 SEM images (inset is the enlarged SEM image) of (a) $CoSn(OH)_6$-Fe0.9%; (b) $CoSn(OH)_6$-Fe1.8%; (c) $CoSn(OH)_6$-Fe2.7%; and (d) $CoSn(OH)_6$-Fe3.8%.

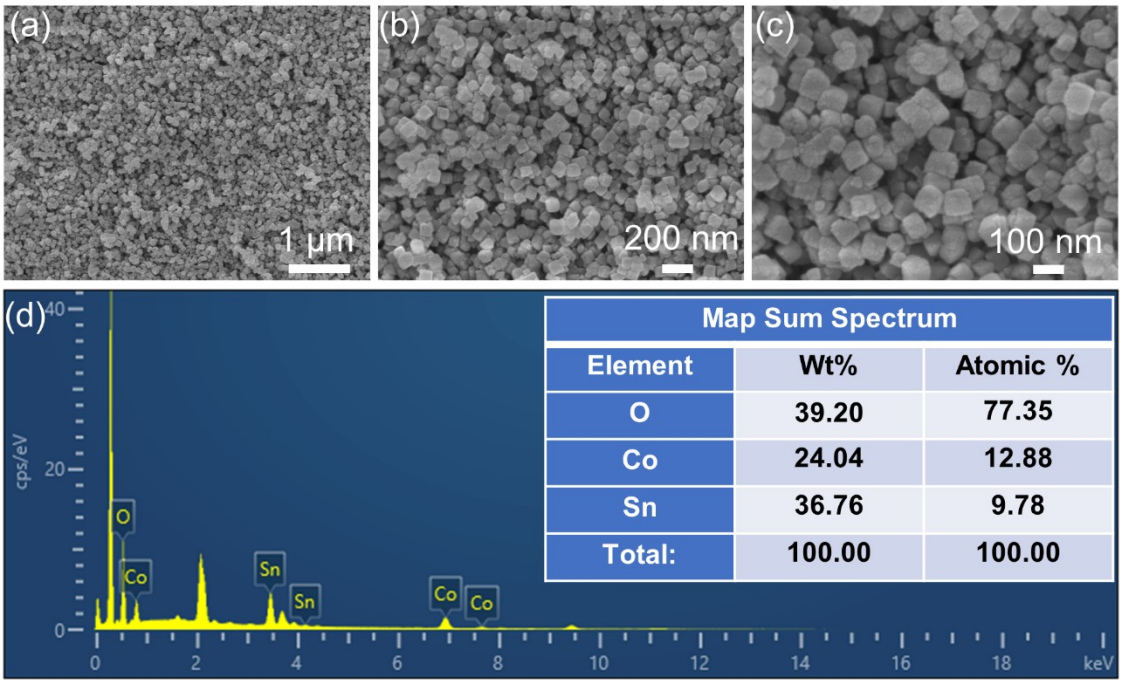

Map Sum Spectrum		
Element	Wt%	Atomic %
O	39.20	77.35
Co	24.04	12.88
Sn	36.76	9.78
Total:	100.00	100.00

Fig. S2 (a-b) SEM images and (c) EDX elecment content result of $CoSn(OH)_6$.

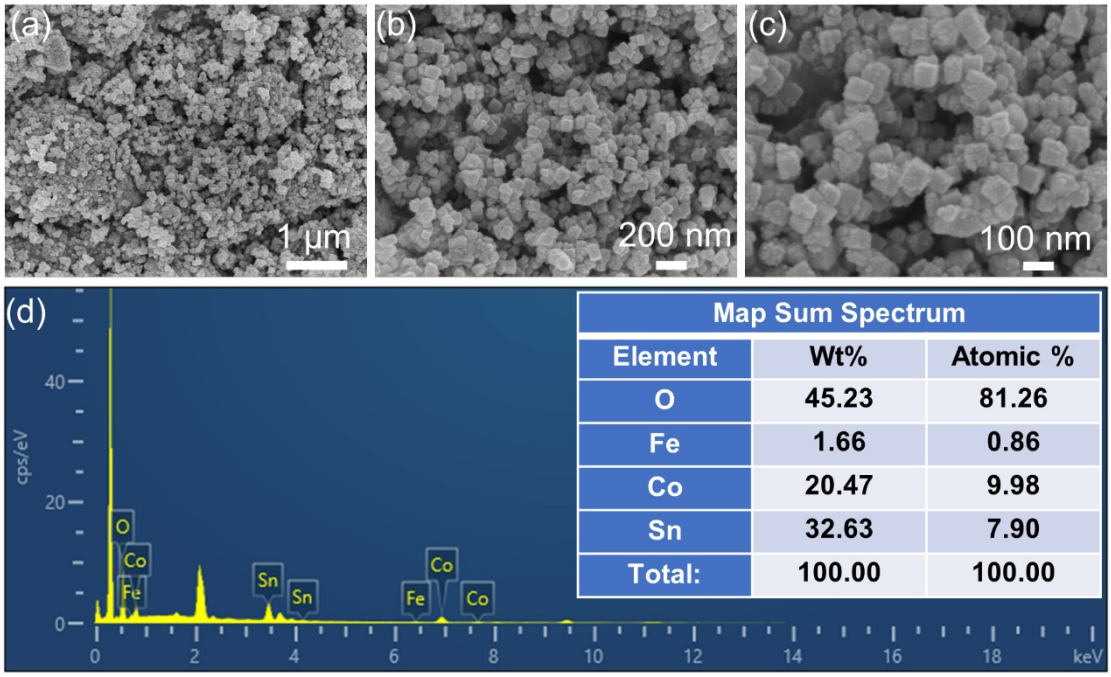

Fig. S3 (a-b) SEM images and (c) EDX elecment content result of $CoSn(OH)_6$-Fe1.8%.

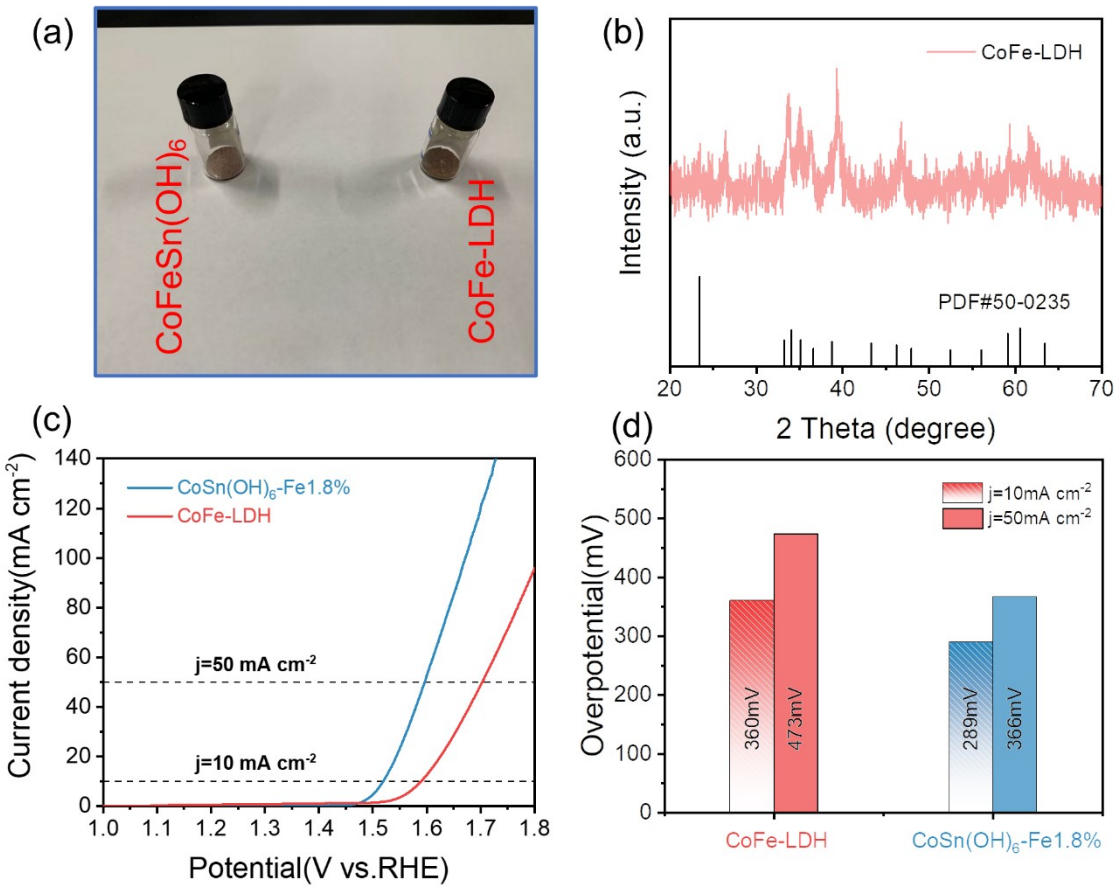

Fig. S4 (a) Photos of the as-prepared materials; (b) XRD pattern of as synthesized CoFe-LDH; OER performance of CoFe-LDH，and $CoSn(OH)_6$-Fe1.8%: (c) LSV curves; and (d) Calculated overpotentials at 10 mA cm^{-2} and 50 mA cm^{-2}.

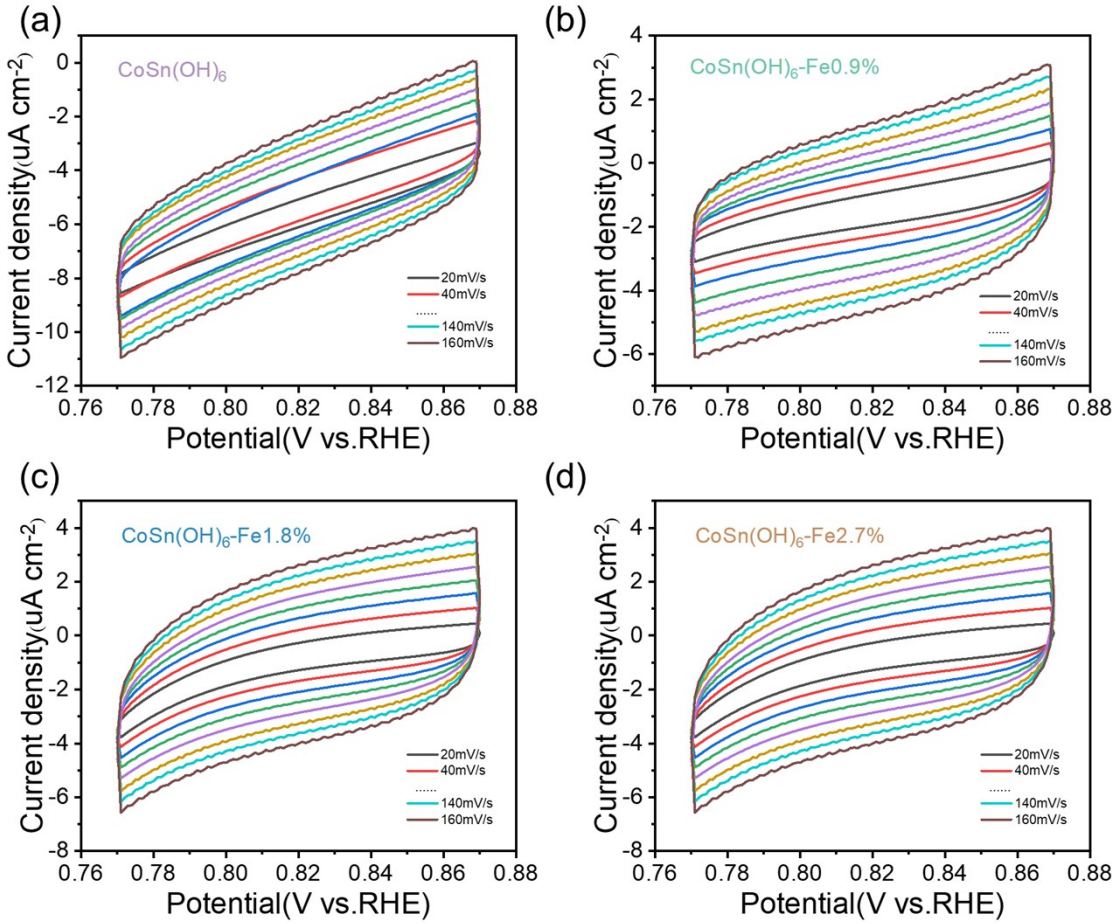

Fig. S5 CV curves of (a) $CoSn(OH)_6$; (b) $CoSn(OH)_6$-Fe0.9%; (c) $CoSn(OH)_6$-Fe1.8%; and (d) $CoSn(OH)_6$-Fe2.7%, with the scan rates of 20, 40, 60, 80, 100,120,140 and 160 mV/s.

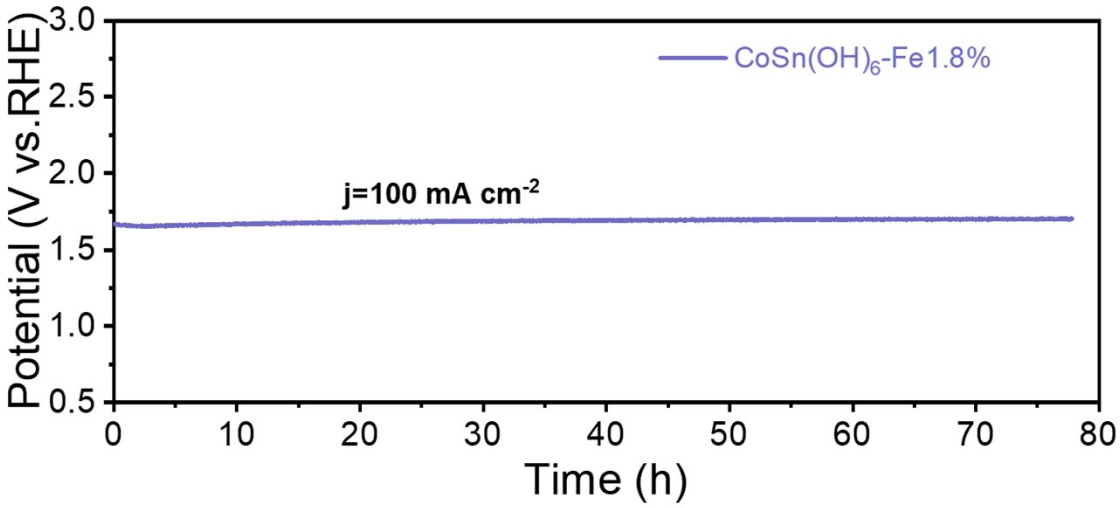

Fig. S6 Chronopotentiometry curves of $CoSn(OH)_6$-Fe1.8% at 100 mA cm^{-2}.

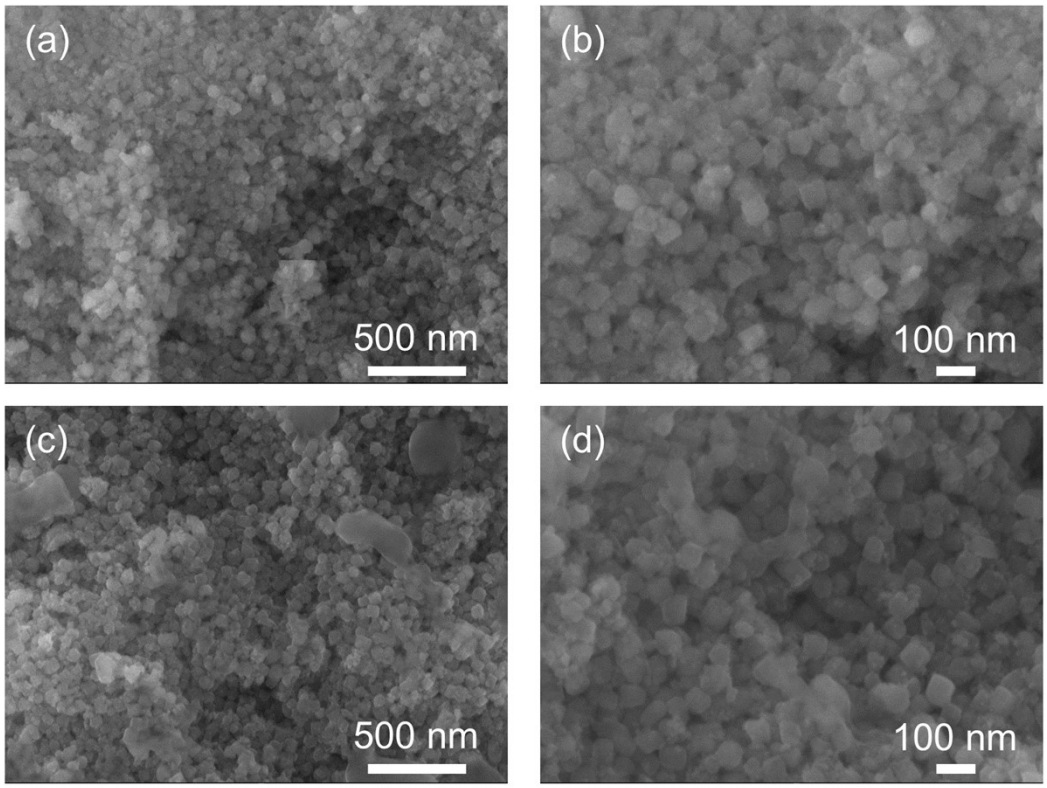

Fig. S7 (a-b) SEM images of $CoSn(OH)_6$-Fe1.8% before the stability measurement; (c-d) SEM images of $CoSn(OH)_6$-Fe1.8% after the stability measurement.

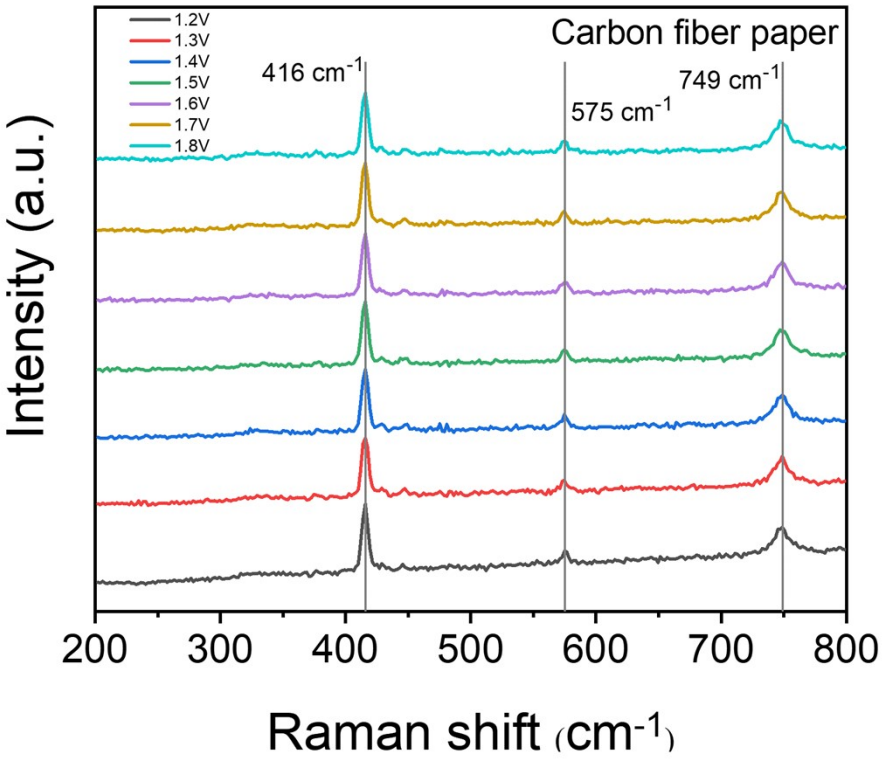

Fig. S8 In-situ Raman spectra of bare carbon fiber paper.

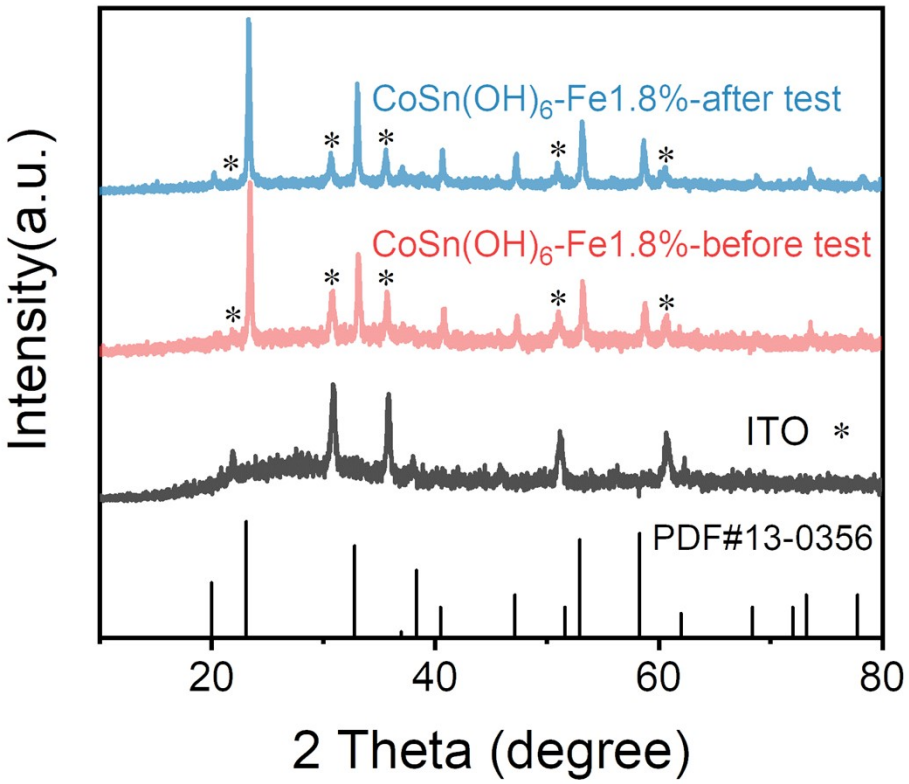

Fig. S9 XRD patterns of $CoSn(OH)_6$-Fe1.8% before and after OER test.

During the XRD inspection process, the peaks of the catalyst material tend to be covered by the peaks of the carbon paper due to the use of carbon paper as a carrier to load the catalyst. In order to better show the difference before and after the electrochemical reaction, ITO glass was chosen as the substrate for the loaded catalyst.

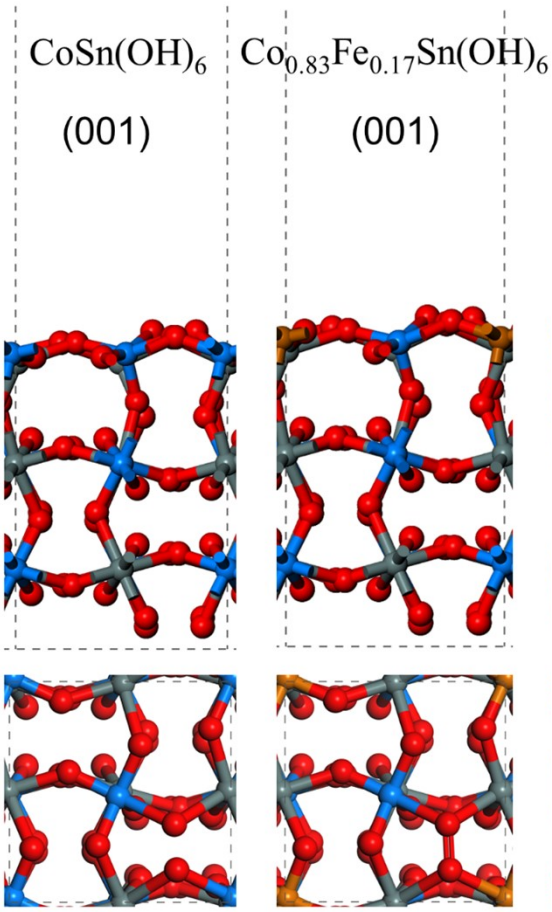

Fig. S10 The atomic models of (001) surface for $CoSn(OH)_6$, and $Co_{0.83}Fe_{0.17}Sn(OH)_6$.

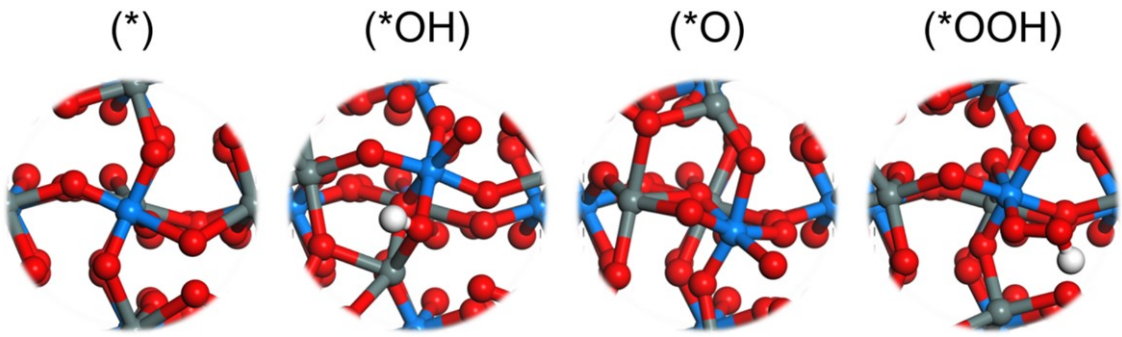

Fig. S11 Adsorption models for various OER steps of $CoSn(OH)_6$.

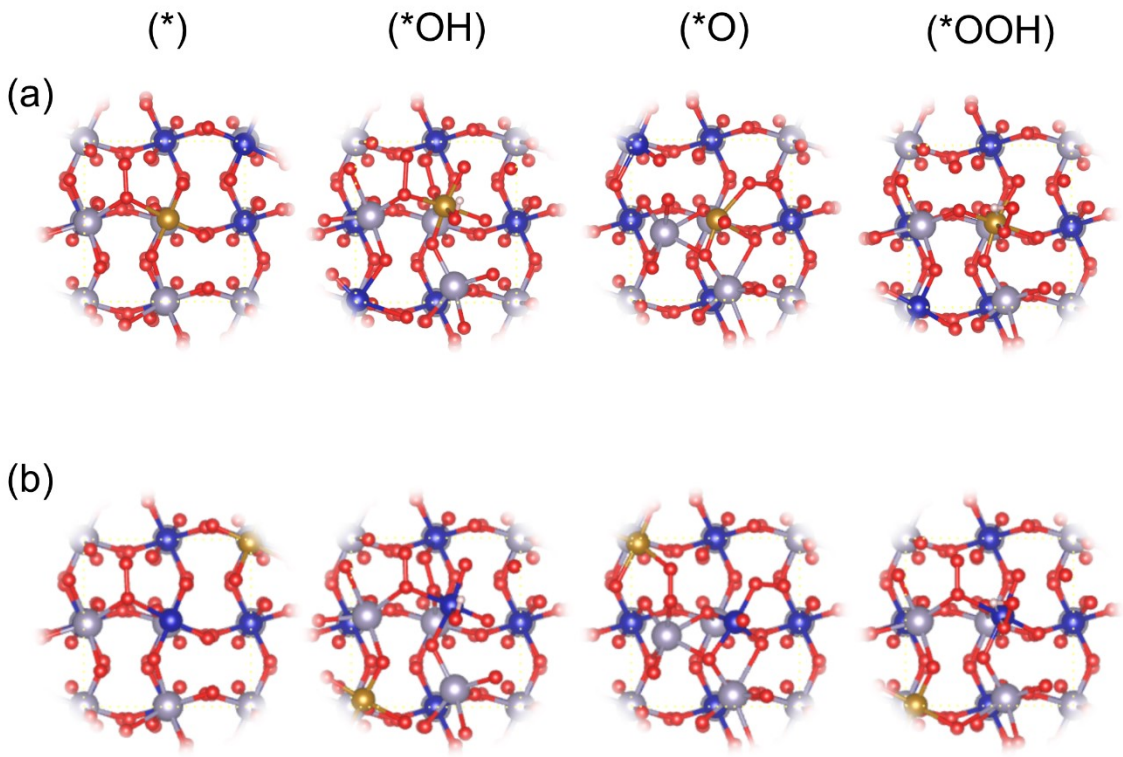

Fig. S12 Adsorption models for various OER steps of $Co_{0.83}Fe_{0.17}Sn(OH)_6$: (a) Fe site; (b) Co site.

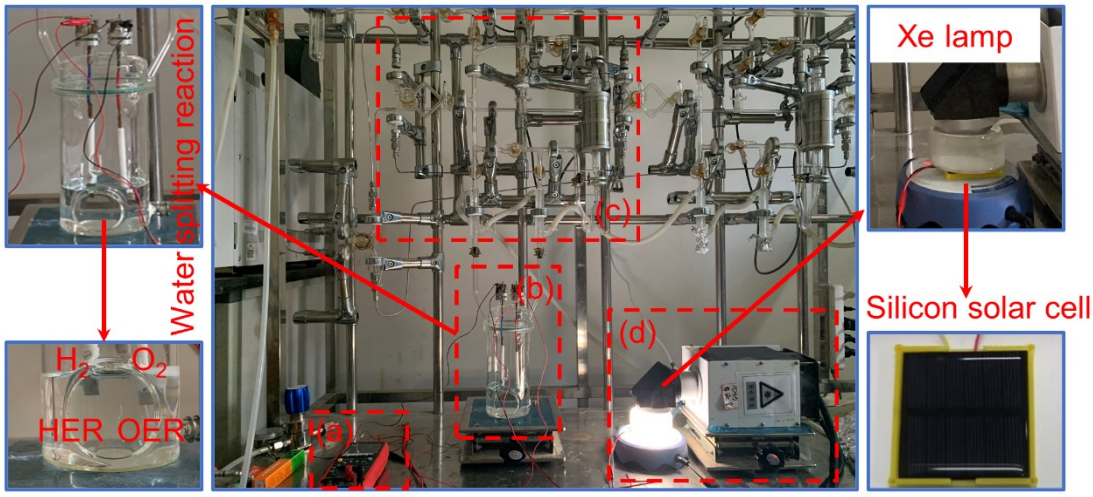

Fig. S13 The photograph of photovoltaic-electrocatalytic water splitting system. (a) A voltmeter; (b) Water splitting reactor; (c) The closed gas-circulation system; (d) Power supply system.

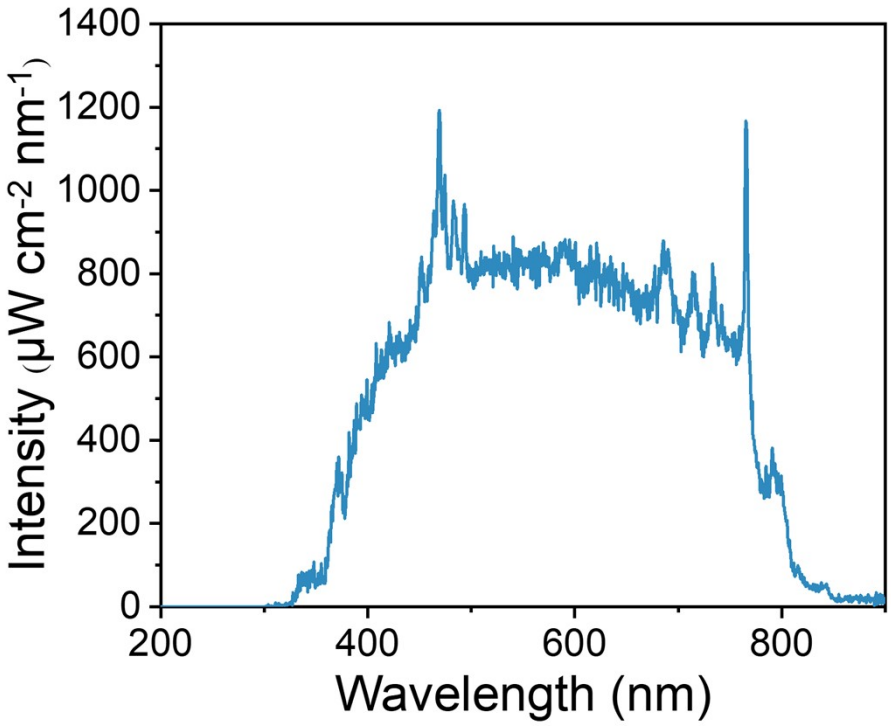

Fig. S14 Irradiative spectrum of the Xe lamp (the major intensity is concentrated on the range of $300 < \lambda < 800$ nm).

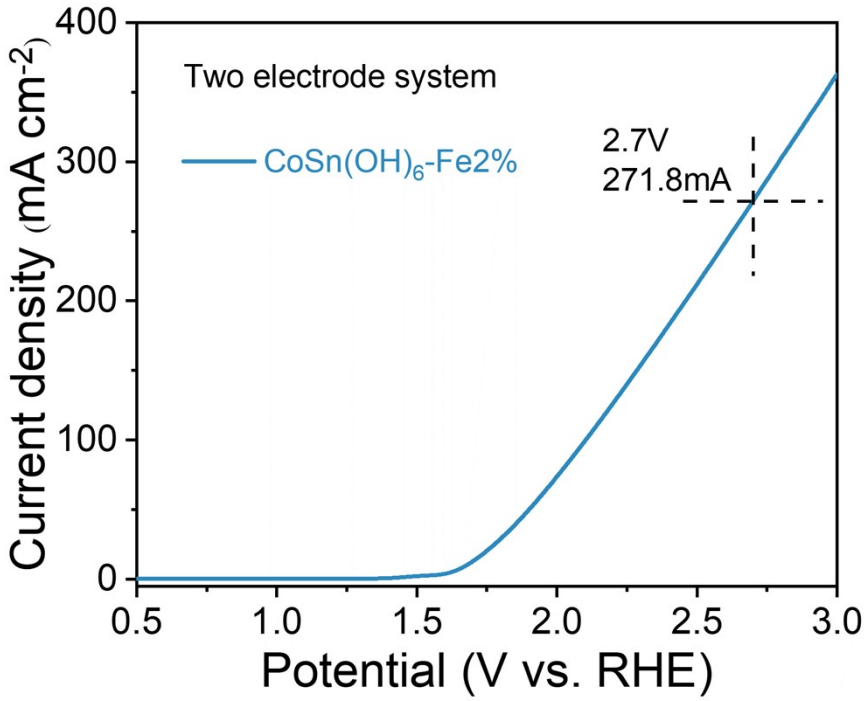

Fig. S15 Linear sweep voltammetry curve of the two-electrode system.

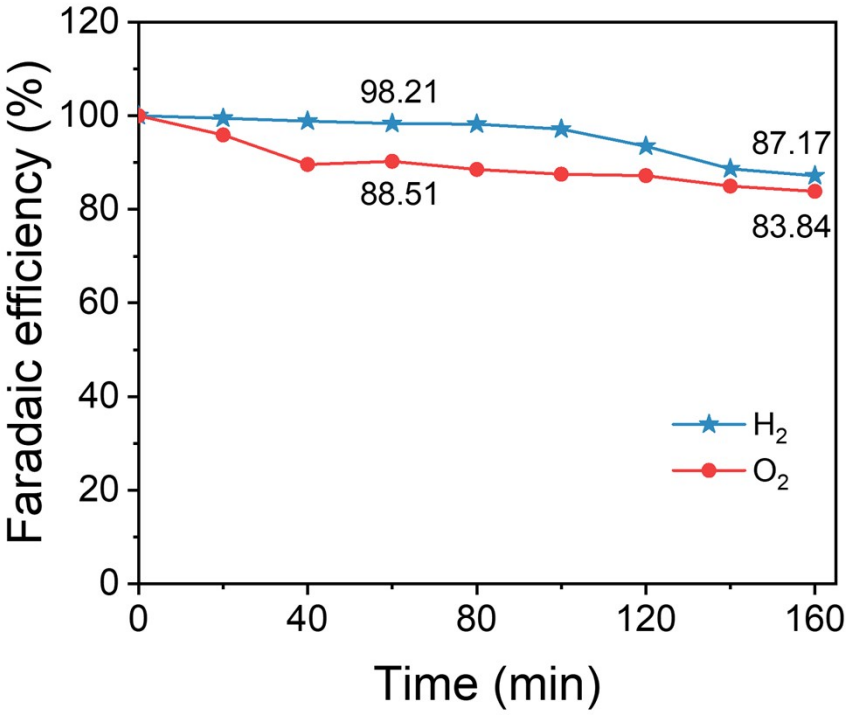

Fig. S16 The calculated Faradaic efficiency.

Table S1 Inductively Coupled Plasma Optical Emission Spectrometer (ICP-OES) elemental content analysis of Fe^{3+} doped $CoSn(OH)_6$.

Sample number	Atomic content		
	Fe	Co	Sn
1	/	21.53%	39.27%
2	0.92%	19.00%	36.00%
3	1.77%	18.09%	35.87%
4	2.69%	16.76%	37.01%

Table S2 The value of Rs and Rct were obtained by fitting the EIS curves.

Products	Rs	Rct
$CoSn(OH)_6$	5.2±0.8	100.8±2.6
$CoSn(OH)_6$-Fe0.9%	6.1±0.3	18.1±0.2
$CoSn(OH)_6$-Fe1.8%	5.1±0.3	11.5±0.1
$CoSn(OH)_6$-Fe2.7%	6.1±0.1	63.2±0.2

Table S3 Comparison between $CoSn(OH)_6$-Fe1.8% and other reported FeCoNi-based catalysts for OER in alkaline electrolyte.

Catalyst	Electrolyte	$\eta^{(a)}$	$T^{(b)}$	Stability	References
$CoSn(OH)_6$-Fe1.8%	1 M KOH	289	54.3	78 h (at 100 mA cm^{-2})	This work
A-FeCoW	1 M KOH	301	70	12 h (at 30 mA cm^{-2})	Ref. 1
FeCoMoW	1 M KOH	212	None	12 h (at 300 mA cm^{-2})	Ref. 2
Co-Fe-N-C	1 M KOH	320	40	4.2 h (at 1 mA cm^{-2})	Ref. 3
CoFe LDH	1 M KOH	404	None	None	Ref. 4
Co-Fe-P nanoboxes	1 M KOH	330	52	16 h (at 50 mA cm^{-2})	Ref. 5
Co(OH)F	1 M KOH	313	52.8	10 h (at 8 mA cm^{-2})	Ref. 6
Fe_3C-Co	1 M KOH	340	None	16.7 h (at 10 mA cm^{-2})	Ref. 7
$SrNb_{0.1}Co_{0.7}Fe_{0.2}O_{3-\delta}$	0.1 M KOH	420	76	After 1000 CV	Ref. 8
$BaCo_{0.7}Fe_{0.2}Sn_{0.1}O_{3-\delta}$	0.1 M KOH	450	69	2 h (at 10 mA cm^{-2})	Ref. 9
Activated $SnCo(OH)_6$	1 M KOH	320	None	13 h (at 5 mA cm^{-2})	Ref. 10
α-$Co(OH)_2$	1 M KOH	340	81	12 h (at 10 mA cm^{-2})	Ref. 11
$Co(OH)_2$@NC	1 M KOH	330	79	After 3000 CV	Ref. 12
ZIF-67@$Co(OH)_2$	1 M KOH	354	73	6 h (at 10 mA cm^{-2})	Ref. 13
Ti/NiO-SnO_2	1 M NaOH	622	53	2 h (at 10 mA cm^{-2})	Ref. 14
Mn_3O_4@SnO_2/Co_3O_4	1 M KOH	420	70.1	After 100 CV	Ref. 15
$Ni_{0.75}Fe_{0.25}(OH)_x$	1 M KOH	310	68	10 h (at 10 mA cm^{-2})	Ref. 16
CoSHN	1 M KOH	358	58.6	2 h (at 10 mA cm^{-2})	Ref. 17
Fe Doped NiO	0.5 M KOH	310	25	2 h (at 10 mA cm^{-2})	Ref. 18
Fe Doped $NiCo_2O_4$	1 M KOH	350	27	After 1000 CV	Ref. 19

(a) overpotential (mV) at current density of 10 mA cm^{-2}; (b) Tafel slope (mV dec^{-1}).

References

1. B. Zhang, X. Zheng, O. Voznyy, R. Comin, M. Bajdich, M. García-Melchor, L. Han, J. Xu, M. Liu, L. Zheng, F. P. García de Arquer, C. T. Dinh, F. Fan, M. Yuan, E. Yassitepe, N. Chen, T. Regier, P. Liu, Y. Li, P. De Luna, A. Janmohamed, H. L. Xin, H. Yang, A. Vojvodic and E. H. Sargent, *Science*, 2016, **352**, 333-337.

2. B. Zhang, L. Wang, Z. Cao, S. M. Kozlov, F. P. García de Arquer, C. T. Dinh, J. Li, Z. Wang, X. Zheng, L. Zhang, Y. Wen, O. Voznyy, R. Comin, P. De Luna, T. Regier, W. Bi, E. E. Alp, C.-W. Pao, L. Zheng, Y. Hu, Y. Ji, Y. Li, Y. Zhang, L. Cavallo, H. Peng and E. H. Sargent, *Nature Catalysis*, 2020, **3**, 985-992.

3. L. Bai, C.-S. Hsu, D. T. L. Alexander, H. M. Chen and X. Hu, *Nature Energy*, 2021, **6**, 1054-1066.

4. F. Dionigi, Z. Zeng, I. Sinev, T. Merzdorf, S. Deshpande, M. B. Lopez, S. Kunze, I. Zegkinoglou, H. Sarodnik, D. Fan, A. Bergmann, J. Drnec, J. F. d. Araujo, M. Gliech, D. Teschner, J. Zhu, W.-X. Li, J. Greeley, B. R. Cuenya and P. Strasser, *Nature Communications*, 2020, **11**, 2522.

5. T. Wang, C. Wang, Y. Jin, A. Sviripa, J. Liang, J. Han, Y. Huang, Q. Li and G. Wu, *Journal of Materials Chemistry A*, 2017, **5**, 25378-25384.

6. S. Wan, J. Qi, W. Zhang, W. Wang, S. Zhang, K. Liu, H. Zheng, J. Sun, S. Wang and R. Cao, *Advanced Materials*, 2017, **29**, 1700286.

7. C. C. Yang, S. F. Zai, Y. T. Zhou, L. Du and Q. Jiang, *Advanced Functional Materials*, 2019, **29**, 1901949.

8. Y. Zhu, W. Zhou, Z.-G. Chen, Y. Chen, C. Su, M. O. Tadé and Z. Shao, *Angewandte Chemie International Edition*, 2015, **54**, 3897-3901.

9. X. Xu, C. Su, W. Zhou, Y. Zhu, Y. Chen and Z. Shao, *Advanced Science*, 2016, **3**, 1500187.

10. F. Song, K. Schenk and X. Hu, *Energy & Environmental Science*, 2016, **9**, 473-477.

11. B. Cao, C. Luo, J. Lao, H. Chen, R. Qi, H. Lin and H. Peng, *ACS Omega*, 2019, **4**, 16612-16618.

12. G. Li, C. Liu, Z. Zhang, B. Cui, Y. Chen, Y. Deng and W. Hu, *Journal of*

Materials Science & Technology, 2021, **81**, 131-138.

13. J.-F. Qin, J.-Y. Xie, N. Wang, B. Dong, T.-S. Chen, Z.-Y. Lin, Z.-Z. Liu, Y.-N. Zhou, M. Yang and Y.-M. Chai, *Journal of Colloid and Interface Science*, 2020, **562**, 279-286.

14. M. Wu, Y. Li, J. Du, C. Tao and Z. Liu, *ACS Omega*, 2020, **5**, 22652-22660.

15. Y. Song, H. Liu, W. Dong and M. Li, *International Journal of Hydrogen Energy*, 2020, **45**, 4501-4510.

16. T. Tian, M. Zheng, J. Lin, X. Meng and Y. Ding, *Chemical Communications*, 2019, **55**, 1044-1047.

17. J. Zhu, S. Li, Z. Zhuang, S. Gao, X. Hong, X. Pan, R. Yu, L. Zhou, L. V. Moskaleva and L. Mai, *Energy & Environmental Materials*, 2022, **5**, 231-237.

18. A. C. Pebley, E. Decolvenaere, T. M. Pollock and M. J. Gordon, *Nanoscale*, 2017, **9**, 15070-15082.

19. K.-L. Yan, X. Shang, Z. Li, B. Dong, X. Li, W.-K. Gao, J.-Q. Chi, Y.-M. Chai and C.-G. Liu, *Applied Surface Science*, 2017, **416**, 371-378.